Research Article | Vol. 8, No. 12 | 1 Dec 2018 | OPTICAL MATERIALS EXPRESS 3887
Optical Materials EXPRESS

# Tunable deflection and asymmetric transmission of THz waves using a thin slab of graphene-dielectric metamaterial, with and without ENZ components

ANDRIY E. SEREBRYANNIKOV,[1,2,*] HODJAT HAJIAN,[3] MIGUEL BERUETE,[4] EKMEL OZBAY,[3,5] AND GUY A. E. VANDENBOSCH[1]

[1]*ESAT-TELEMIC, Katholieke Universiteit Leuven, 3001 Leuven, Belgium*
[2]*Faculty of Physics, Adam Mickiewicz University, 61-614 Poznań, Poland*
[3]*NANOTAM - Nanotechnology Research Center, Bilkent University, 06800 Ankara, Turkey*
[4]*Antennas Group - TERALAB and Institute of Smart Cities, Universidad Pública de Navarra, 31006 Pamplona, Spain*
[5]*Department of Physics, Department of Electrical Engineering, UNAM - National Institute of Materials Science and Nanotechnology, Bilkent University, 06800 Ankara, Turkey*
[*]*andser@amu.edu.pl*

**Abstract:** Tunable deflection of obliquely incident, linearly polarized terahertz waves is theoretically studied in a wide frequency range around 20 THz, by combining a thin slab of graphene-dielectric metamaterial (with ten layers of graphene), a dielectric grating, and a uniform polar-dielectric slab operating in the epsilon-near-zero (ENZ) regime. The modulation of the deflection intensity and deflection angle is done by varying the chemical potential of graphene, and is realized with or without connection to the asymmetric transmission. It is shown to depend on the location of the graphene-dielectric metamaterial slab, as well as on the incidence angle. Four scenarios of tunable deflection are found, including the ones realizable in two-component structures without an ENZ slab.



## 1. Introduction

The last decade has witnessed an unprecedented progress in actively tunable microwave, terahertz, and optical devices and structures thanks to the advent of graphene [1–3]. Being one-atom thick and efficiently tunable by varying the chemical potential, single-layer graphene shows a dynamically changeable conductivity, permittivity, and impedance [4]. So far, the focus of research has been put on single-layer uniform and patterned graphene [1,5–9], which is the simplest case for experimental studies. However, double-layer graphene [10] and graphene-dielectric multilayers [1,11–14] provide more flexibility for tunable devices. Among the new perspectives opened with graphene-dielectric multilayer structures, hyperbolic metamaterials [12,15–20], tunable beam steering [14], and Tamm surface plasmons [13] stand out. Besides, surface-plasmon-polaritons at the interfaces of nanostructured metamaterials containing graphene [21], tunable surface waves at the interface separating different graphene-dielectric hyperbolic metamaterials [22], and tunable perfect absorption at mid-infrared frequencies [23] should be mentioned. It is noteworthy that dispersion of graphene-dielectric metamaterials can be tuned by modifying the Fermi energy, e.g., see Refs. [15,19]. The simplest regime is when equifrequency dispersion contours in the plane of layers are circular, i.e., dispersion is isotropic. Both single-layer graphene and properly designed graphene-dielectric metamaterials show a transition from plasmonic to dielectric state with isotropic-type dispersion, so they may be utilized as tunable components with epsilon-near-zero (ENZ) behavior [11]. Recent experimental demonstration of the metamaterial with five graphene layers and five dielectric layers [24] has opened a route towards the practical realization of many

#340164 https://doi.org/10.1364/OME.8.003887
Journal © 2018 Received 19 Jul 2018; revised 7 Sep 2018; accepted 28 Sep 2018; published 26 Nov 2018

Optical Materials EXPRESS

ideas related to multilayer structures that have been suggested during the last years.

Tunable metamaterials are expected to significantly enhance the performance and functionality of deflection devices and asymmetric transmission devices. Asymmetric transmission is a general Lorentz-reciprocal phenomenon, which is observed when a structure with broken structural symmetry is illuminated by identical waves from the two opposite incidence directions [25–32]. It manifests itself in that transmission may strongly differ for two opposite directions of incidence, and even vanish for one of them. This behavior originates from the difference in coupling conditions at the two interfaces that can be considered in terms of the generalized mode conversion. The simplest way to obtain efficient wideband deflections is connected with the common effect of diffraction and dispersion. It can lead to a strong asymmetry in transmission, due to re-distribution of the incident-wave energy in favor of higher diffraction orders. They are necessarily *deflected* from the both incidence and specular-reflection directions, while the opposite-side transmission is blocked, e.g., by using (meta-)materials with ENZ behavior [33–37]. A purely diffractive mechanism enables deflections [32, 38] but does not ensure such a blocking.

Recently, single-layer graphene has been used in the structures, in which asymmetric transmission is achieved by the mechanisms different from the above-mentioned ones, i.e., by enforcing a change of polarization state with [39] or without [40–43] deflection. Efficient tuning of deflection is possible using thick slabs of graphene-dielectric metamaterial, but it needs a sophisticated design and several hundreds of graphene-dielectric layers [14].

In this paper, we demonstrate electrically tunable deflection of obliquely incident, linearly polarized plane electromagnetic waves in the frequency range around 20 THz, in the framework of the combined diffraction-dispersion mechanism of asymmetric transmission, like in Refs. [29, 34, 35], and in the framework of the purely diffractive mechanism of asymmetric transmission, like in Refs. [32, 38], by using just ten periods of a graphene-dielectric metamaterial. The main goal of this paper is to demonstrate the principal possibility and find various scenarios of dynamical tuning of deflection, which is expected to be achievable by varying the chemical potential of graphene, $\mu$. Deflection and asymmetry in transmission are obtained in the studied structures by means of re-distribution of the incident-wave energy in favor of the diffraction order $m = -1$, similarly to Refs. [26, 35]. We consider the both, i.e., dispersion-diffraction and purely diffraction based machanisms. In the former, the wideband blocking of zero-order transmission by ENZ slab is exploited [35]. In the latter, a weakening of zero order is rather of accidental nature. The changes in response of the studied structures are observed while varying $\mu$ from 0.01 eV to 0.7 eV, in a rather wide frequency range, at the selected values of incidence angle, $\theta$. Optimization of design, e.g., in terms of practical limitations, feasibility, efficiency, etc., is beyond the scope of this paper, and will be considered at the next steps of this research program. The focus here is demonstration of the main features. The presented results are obtained by using the coupled-integral-equation technique [44]. The simulations are performed by using a custom-made MATLAB code, which is based on the fast iterative solution of the coupled integral equations in the frequency domain by using pre-conditioning. The code has been used in the studies of various periodic structures, so its accuracy and convergence features are well known.

## 2. Material properties and design

The studied structure contains, in the general case, three components [Fig. 1(a)]: grating made of Si ($\varepsilon = \varepsilon_g = 12.25$), a slab of graphene-dielectric metamaterial, and a uniform slab of a material with ENZ behavior. The first component is responsible for the creation of higher-order transmission channel(s), for which the coupling of the incident waves differs for the two opposite interfaces. The second one is assumed to have just ten graphene and ten dielectric layers. Its role is to attain tunability by changing the state from dielectric to ENZ, and then to plasmonic one, by increasing $\mu$ [11]. The third component's role is to block zero-order transmission in ENZ regime, $t_0 = t_0^{\rightarrow} = t_0^{\leftarrow} = 0$, as well as first-order transmission but only for one of the two

Optical Materials EXPRESS

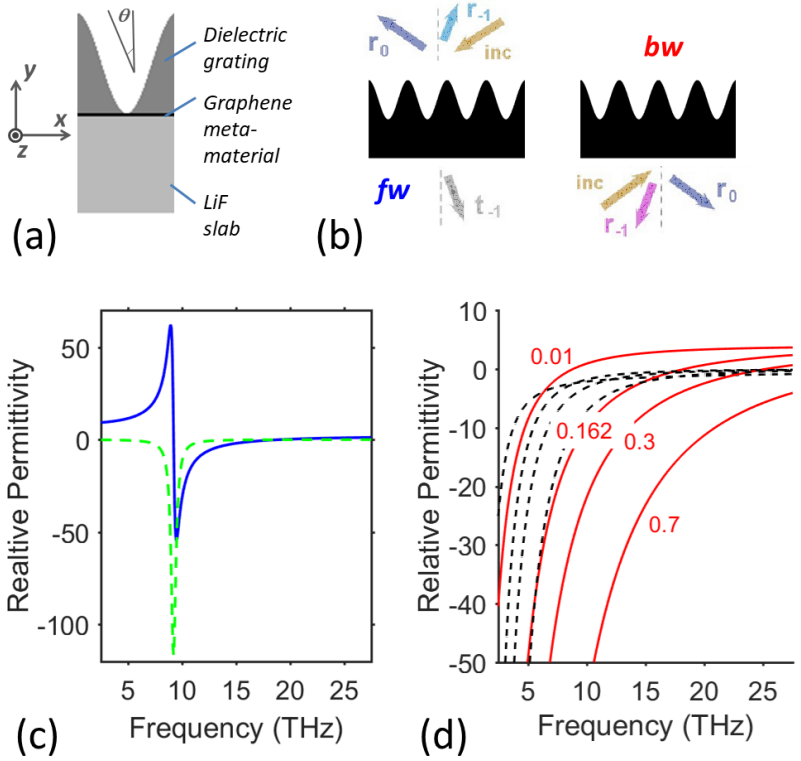


Fig. 1. (a) Geometry of a single period of the studied structure; (b) Schematic showing connection between deflection and asymmetric transmission; $r_{-1}, t_{-1}$, and $r_0$ denote reflection and transmission of the order $m = -1$ and reflection of the order $m = 0$, respectively; *fw* and *bw* stand for forward and backward illumination cases; (c) Permittivity of LiF, $\varepsilon_{LiF}$, $\mathrm{Re}(\varepsilon_{LiF})$ - solid blue line, $\mathrm{Im}(\varepsilon_{LiF})$ - dashed green line; (d) Permittivity of graphene-dielectric metamaterial, $\mathrm{Re}(\varepsilon^{gm}_{(xx)})$ - solid red lines and $\mathrm{Im}(\varepsilon^{gm}_{(xx)})$ - dashed black lines; numbers near curves give values of $\mu$ in eV.

incidence directions, e.g., either $t^{\leftarrow}_{-1} = 0$ or $t^{\rightarrow}_{-1} = 0$, in a desired range of $\theta$ [33–35]. Signs $\rightarrow$ and $\leftarrow$ stand for the forward, i.e., grating-side, and the backward, i.e., noncorrugated-side illumination, respectively [see Fig. 2(b)]. The outgoing wave's direction for $m = -1$ is given by the grating theory as follows [45]:

$$\phi_{-1} = \arcsin(\sin\theta - 2\pi/kL), \tag{1}$$

where $k = \omega/c$, $\omega = 2\pi f$ is angular frequency, $f$ is frequency, $c$ is the velocity of electromagnetic wave, and $L$ is the grating period. The deflection angle for transmitted waves, $\phi_m$, $|m| > 0$, is measured from the vertical dashed line in clockwise direction in Fig. 1(b). In the operation regimes considered in Section 3, we have only two propagating orders, $m = 0$ and $m = -1$, while the first of them can be fully suppressed by the ENZ slab. Moreover, an accidental weakening of zero order is possible without an ENZ slab.

There are various natural materials that show ENZ behavior at THz frequencies. In particular, they include polar dielectrics (PDs), which are strongly dispersive at THz fequencies due to the coupling of transverse phonon-photon resonances [46]. This gives rise to a frequency range with the real part of permittivity that is larger than zero but smaller than unity, which is located right above the polaritonic gap (Reststrahlen band). The natural behavior of PDs at THz enables many

Optical Materials EXPRESS

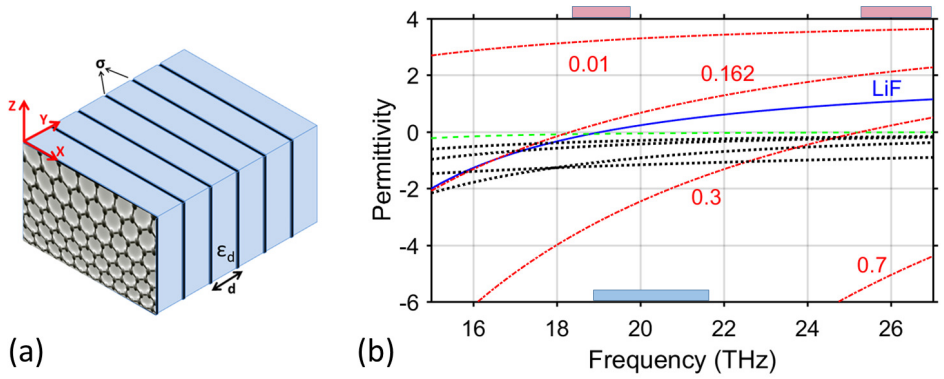


Fig. 2. (a) Schematic of the layered graphene-dielectric metamaterial. Six layers of graphene and six dielectric layers are shown here; (b) Permittivity of LiF, $\varepsilon_{LiF}$, and graphene-dielectric metamaterial, $\varepsilon^{gm}_{(xx)}$ in the studied frequency range: Re($\varepsilon_{LiF}$) - solid blue line, Im($\varepsilon_{LiF}$) - dashed green line; Re($\varepsilon^{gm}_{(xx)}$) - dash-dotted red lines and Im($\varepsilon^{gm}_{(xx)}$) - dotted black lines; numbers at the red lines mean $\mu$ in eV; rectangular rose bars at the plot top approximately indicate location of the range of $0 < \mathrm{Re}(\varepsilon^{gm}_{(xx)}) < 0.5$ at $\mu = 0.162$ eV and $\mu = 0.3$ eV; rectangular blue bar at the plot bottom approximately indicates location of the range of $0 < \mathrm{Re}(\varepsilon_{LiF}) < 0.5$.

interesting phenomena, even when using uniform slabs of these materials [33,47]. This variety can be further extended by using periodic structures and components made of PDs , e.g., see Refs. [48–51]. In this paper, the consideration is restricted to the case when the PD slab is made of LiF, whose complex permittivity is given as follows:

$$\varepsilon_{LiF} = \varepsilon_\infty + (\varepsilon_0 - \varepsilon_\infty)\omega_T^2/(\omega_T^2 - \omega^2 + i\Gamma\omega), \tag{2}$$

where $\varepsilon_\infty = 2.027$ is the high-frequency permittivity, $\varepsilon_0 = 8.705$ is static permittivity, $\omega_T$ is the transverse phonon resonance frequency, and $\Gamma$ is the absorption factor; $\omega_T/(2\pi) = 9.22$ THz and $\Gamma = 0.527$ THz [48,52]. Assuming $\Gamma = 0$, the lower and upper boundaries of the polaritonic gap are set by the transverse ($\omega_T$) and longitudinal ($\omega_L$) phonon resonance frequencies, in line with the Lyddane-Sachs-Teller relation, $\omega_L^2/\omega_T^2 = \varepsilon_0/\varepsilon_\infty$ [46]. These boundaries are slightly different when $\Gamma > 0$ is taken into account. LiF has a wide range of $0 < \mathrm{Re}(\varepsilon_{LiF}) < 1$ above the polaritonic gap, i.e., at $19.1 < f < 25.2$ THz. Permittivity of LiF is presented in Fig. 1(c). In the simplified version of the studied structure, the LiF slab with ENZ behavior is absent.

The graphene-dielectric metamaterial represents ten layers of graphene that are separated by ten layers of dielectric, similarly to Fig. 2(a). Conductivity of graphene is given by $\sigma = \sigma^{intra} + \sigma^{inter}$ with [4]

$$\sigma^{intra} = \frac{e^2}{4\hbar}\frac{i}{2\pi}\left\{\frac{16k_BT}{\hbar\Omega}\ln\left(2\cosh\left(\frac{\mu}{2k_BT}\right)\right)\right\}, \tag{3}$$

$$\sigma^{inter} = \frac{e^2}{4\hbar}\frac{1}{2} + \frac{e^2}{4\hbar}\frac{1}{\pi}\arctan\left(\frac{\hbar\Omega - 2\mu}{2k_BT}\right) - \frac{e^2}{4\hbar}\frac{i}{2\pi}\ln\frac{(\hbar\Omega + 2\mu)^2}{(\hbar\Omega - 2\mu)^2 + (2k_BT)^2}, \tag{4}$$

where $e$ is the electron charge, $\hbar$ is the Plank constant over $2\pi$, $k_B$ is the Boltzmann constant, $T$ is temperature, $\Omega = \omega + i\tau^{-1}$, and $\tau$ is relaxation time. It is assumed here that $T = 300$ K and $\tau = 0.135$ ps. Such a metamaterial effectively represents a uniaxial anisotropic material with nonzero diagonal components of the permittivity tensor and zero nondiagonal components. At

Optical Materials EXPRESS

a proper choice of the parameters of the dielectric layers, the components of the metamaterial permittivity tensor, $\varepsilon^{gm}_{(xx)}$, $\varepsilon^{gm}_{(yy)}$, and $\varepsilon^{gm}_{(zz)}$, can be obtained by using the effective medium theory as follows [11]:

$$\varepsilon^{gm}_{(xx)} = \varepsilon^{gm}_{(zz)} = \varepsilon_d - i\sigma/(\omega\varepsilon_0 d), \tag{5}$$

$$\varepsilon^{gm}_{(yy)} = \varepsilon_d, \tag{6}$$

where $\varepsilon_0$ is the permittivity of free space, $\sigma$ is conductivity of graphene, $d$ and $\varepsilon_d$ are thickness and permittivity of the dielectric layer (spacer), respectively. The effective permittivity $\varepsilon^{gm}_{(xx)}$ is plotted in Fig. 1(d) for the case of $d = 38.2$ nm and $\varepsilon_d = 4$, which is studied in detail in this paper. This choice allows us to obtain $0 < \mathrm{Re}(\varepsilon^{gm}_{(xx)}) < 0.5$ when $0 < \mathrm{Re}(\varepsilon_{LiF}) < 1$, and, thus, avoid strong mismatches in permittivity values between the LiF slab and the graphene-dielectric metamaterial slab at the properly selected $\mu$, see Fig. 2(b). Since only circular equifrequency dispersion contours occur in the framework of the used model of metamaterial, the theory developed in Ref. [35] is fully applicable. Therefore, we do not present here details of dispersion analysis.

One can see that $\mathrm{Re}\varepsilon^{gm}_{(xx)}$ crosses zero at a frequency which depends on $\mu$. For instance, this happens at 8.85 THz when $\mu = 0.01$ eV, and at 25.3 THz when $\mu = 0.3$ eV. Consequently, spectral location of the region of transition from the effectively plasmonic to the effectively dielectric state can be significantly shifted by means of variations in $\mu$. Note that the gate positioning will be considered at the next steps. Generally, electrical gating of a multilayer graphene-dielectric metamaterial is a challenging task. One of possible gating schemes is presented in Ref. [11]. In Ref. [24], chemical doping has been used while preparing each graphene layer using CVD, instead of electrical gating. In Ref. [53], the double-layer graphene has been experimentally gated, and the method was presented by the authors as the one being usable for the structures composed of a larger number of graphene monolayers. So, from a practical point of view, this approach can be utilized also in the case of graphene-dielectric metamaterial that contains ten layers of graphene, like that one in our study.

The grating shape is set by

$$y = (t_{Si}/2)[1 + \cos(2\pi x/L)], \tag{7}$$

where $L = 9.55$ $\mu$m and $t_{Si} = L$ is the grating thickness. The thickness of the LiF slab is $t_{LiF} = 9.17$ $\mu$m, and the thickness of the graphene-dielectric metamaterial slab is $t_{gm} = 382$ nm. The incident plane wave is assumed to be linearly polarized, with electric-field vector parallel to $z$-axis.

## 3. Results and discussion

We compare three configurations, two of which contain the ENZ (here - LiF) uniform slab but differ in location of the graphene-dielectric metamaterial slab, and one configuration without the ENZ slab. In this paper, consideration is restricted to the case when transmission is calculated after homogenization.

### 3.1. Structures with LiF slab

In the *first configuration*, the metamaterial slab is located below the ENZ slab, i.e., at the interface opposite to the grating. In the *second configuration*, it is sandwiched between the grating and the ENZ slab, as shown in Fig. 1(a). For demonstration purposes, we selected two values of $\theta$, 60° and 82°, for which adjustment of the structural parameters is not complicated. The obtained results indicate that the structure can be re-designed to operate at smaller $\theta$. Besides, there is freedom in the choice of the grating material and ENZ slab material. Figure 3 presents the calculated zero-order ($m = 0$) and first-order ($m = -1$) transmittances for the first configuration.

Optical Materials EXPRESS

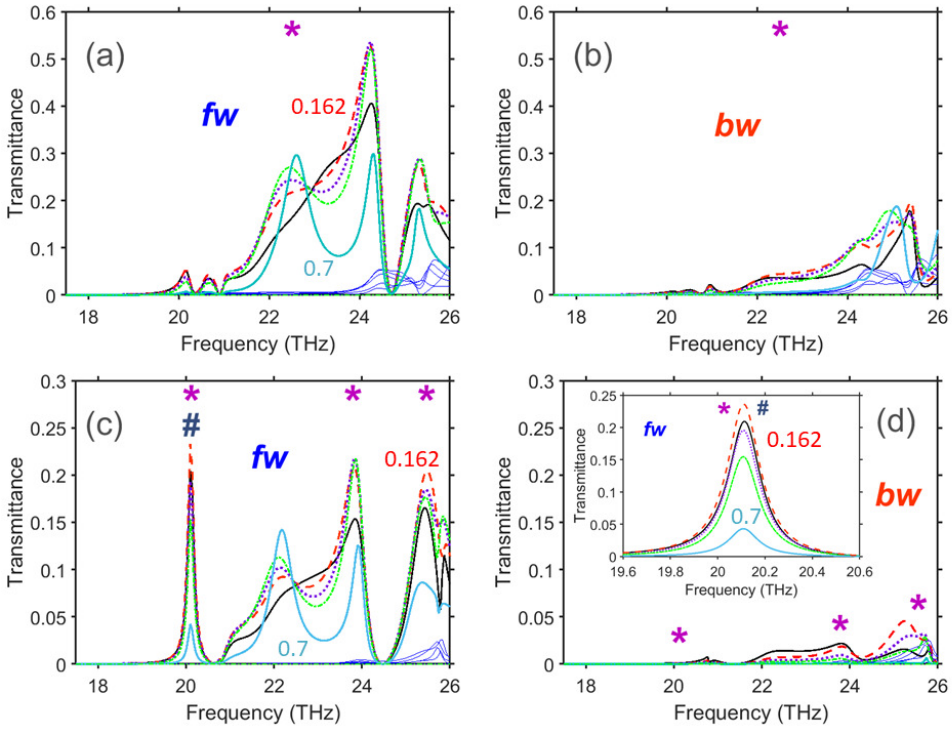


Fig. 3. (a) First-order forward-case transmittance, $t_{-1}^{\rightarrow}$, at $\theta = 60°$; (b) first-order backward-case transmittance, $t_{-1}^{\leftarrow}$, at $\theta = 60°$; (c) first-order forward-case transmittance, $t_{-1}^{\rightarrow}$, at $\theta = 82°$; (d) first-order backward-case transmittance, $t_{-1}^{\leftarrow}$, at $\theta = 82°$; solid black line - $\mu = 0.01$ eV, dashed red line - $\mu = 0.162$ eV; dotted violet line - $\mu = 0.23$ eV; dash-dotted green line - $\mu = 0.3$ eV; solid light-blue line - $\mu = 0.7$ eV; thin solid dark-blue lines - zero-order transmittance, $t_0 = t_0^{\rightarrow} = t_0^{\leftarrow}$ (nonzero mainly at $f > 24$ THz); graphene metamaterial is located below the LiF slab; inset in plot (d) shows fragment of plot (c); *fw* and *bw* stand for forward and backward cases; asterisks and number signs indicate spectral location of some of the regimes of tunable asymmetric transmission and tunable deflection, respectively. Numbers near some of the curves indicate $\mu$ in eV (in the same color as the curves).

There is a strong asymmetry in transmission for both $\theta = 60°$ and $\theta = 82°$, as seen from the comparison of Fig. 3(a) with Fig. 3(b), and Fig. 3(c) with Fig. 3(d), respectively.

In Fig. 3(a,b) plotted for $\theta = 60°$, $t_{-1}^{\rightarrow}$ dominates over $t_0$ at least at $20 < f < 24$ THz, i.e., transmission is mainly due to the deflected, $m = -1$ order beam. $t_{-1}^{\rightarrow}$ is several times larger than $t_{-1}^{\leftarrow}$ giving evidence of the so-called direct regime of asymmetric transmission. At the same time, the so-called inverse regime [54] is obtained at $f = 24.4$ THz, where $t_{-1}^{\leftarrow}$ is significantly larger than $t_{-1}^{\rightarrow}$. Sensitivity to variations in $\mu$ at $\theta = 60°$ is moderate, with a 3.5-fold difference in $t_{-1}^{\rightarrow}$ at 23.6 THz, while $\mu$ is varied from 0.01 eV to 0.7 eV, and a 3.1-fold difference at 24 THz, while $\mu$ is varied from 0.162 eV to 0.7 eV.

The situation is different for $\theta = 82°$, see Fig. 3(c,d). Here, we obtain a peak of $t_{-1}^{\rightarrow}$ at 20 THz ($\phi_{-1} = -35.5°$), whose location does not depend on $\mu$, but the magnitude strongly depends on it. There is a nearly five-fold difference in $t_{-1}^{\rightarrow}$ between the cases of $\mu = 0.01$ eV and $\mu = 0.7$ eV. Since $t_{-1}^{\leftarrow} \approx 0$ at 20 THz, the peak of $t_{-1}^{\rightarrow}$ is a tunable asymmetric-transmission peak, so that tunable deflection is realized here at $\phi_{-1} = \text{const}$ by changing the magnitude with $\mu$. One can see that the capability of the slab of graphene-dielectric metamaterial as a tunable component in the studied structure depends on $\theta$. Variations in $\theta$ may give an additional degree of freedom,

Optical Materials EXPRESS

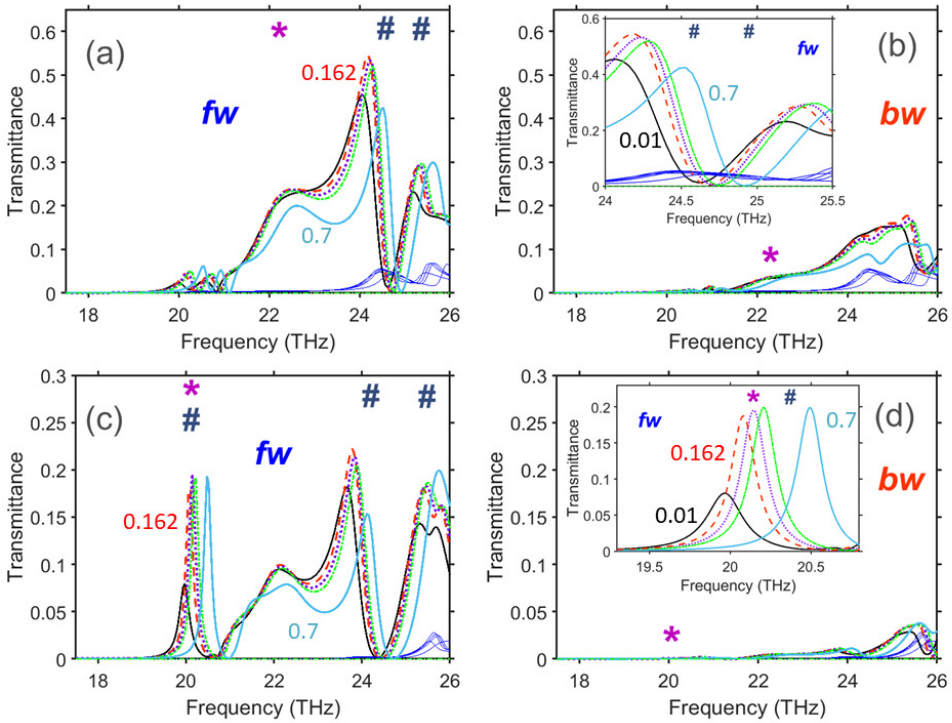


Fig. 4. First-order forward-case transmittance, $t_{-1}^{\rightarrow}$, at $\theta = 60°$; (b) first-order backard-case transmittance, $t_{-1}^{\leftarrow}$, at $\theta = 60°$; (c) first-order forward-case transmittance, $t_{-1}^{\rightarrow}$, at $\theta = 82°$; (d) first-order backward-case transmittance, $t_{-1}^{\leftarrow}$, at $\theta = 82°$; solid black line - $\mu = 0.01$ eV, dashed red line - $\mu = 0.162$ eV; dotted violet line - $\mu = 0.23$ eV; dash-dotted green line - $\mu = 0.3$ eV; solid light-blue line - $\mu = 0.7$ eV; thin solid dark-blue lines - zero-order transmittance, $t_0 = t_0^{\rightarrow} = t_0^{\leftarrow}$ (nonzero mainly at $f > 24$ THz); slab of graphene-dielectric metamaterial is located between the Si grating and the LiF slab, as shown in Fig. 1(a); insets in plots (b), (d) are fragments of plots (a), (c), respectively; *fw*, *bw*, and asterisks and number signs have the same meaning as in Fig. 3. Numbers near some of the curves indicate $\mu$ in eV (in the same color as the curves).

enabling for instance the switching between asymmetric transmission / deflection regime and two-side reflection at fixed $f$ and $\mu$.

Now, let us consider the *second configuration*, in which the metamaterial slab is located between the Si grating and the LiF slab. Figure 4 presents the results in a similar manner as Fig. 3. While most of the features observed in Fig. 3(a,b) for 60° are kept in Fig. 4(a,b), there is one new and very important feature. The right edge of the lowest high-transmission range (at $f = 24.5$ THz, $\phi_{-1} = -24.6°$) is now shifted while $\mu$ is varied. This enables both gradual tuning (optimally, at 24.6 THz) and on-off switching (e.g., at 24.6 and 24.9 THz) of the deflected beam by varying $\mu$. For example, at $f = 24.6$ THz, we obtain $t_{-1}^{\rightarrow} = 0.375$ for $\mu = 0.7$ eV and $t_{-1}^{\rightarrow} = 0.015$ for $\mu = 0.01$ eV. At $f = 24.9$ THz, the situation is opposite, i.e., $t_{-1}^{\rightarrow} = 5 \times 10^{-3}$ for $\mu = 0.7$ eV and $t_{-1}^{\rightarrow} = 0.13$ for $\mu = 0.01$ eV. It is worth noting that asymmetry in transmission is not strong in this case, because of the significant contribution of $t_0$ and $t_{-1}^{\leftarrow}$.

Figure 4(c,d) presents the results for $\theta = 82°$. The peak of $t_{-1}^{\rightarrow}$ in the vicinity of 20 THz is similar to that in Fig. 3(c,d) at 20 THz, but now its spectral location depends on $\mu$. Furthermore, a new scenario can be obtained, in which the peaks are just weakly overlapped at different values

Optical Materials EXPRESS

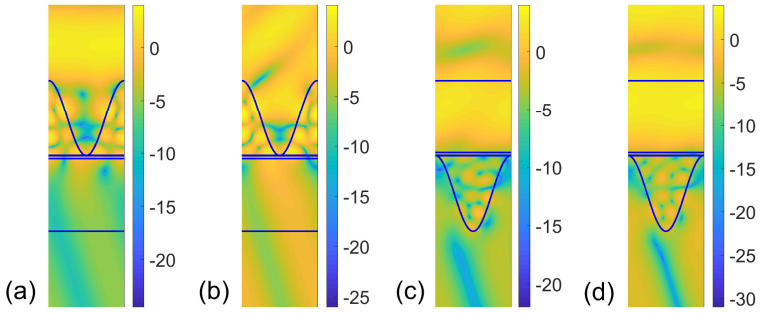


Fig. 5. Electric field distribution within one period of the structure, in which the slab of metamaterial is located between the Si grating and the LiF slab, at $f = 24.57$ THz and $\theta = 60°$, (a) $\mu = 0.01$ eV and (b) $\mu = 0.7$ eV at forward-case illumination, and (c) $\mu = 0.01$ eV and (d) $\mu = 0.7$ eV at backward-case illumination. Solid lines show location of the structural components.

of $\mu$. In the vicinity of 24.5 THz, the scenario of tunable deflection, which has been discussed above for 60° in Fig. 4(a,b), remains also for 82° in Fig. 4(c,d) ($\phi_{-1} \approx -17°$), but a smaller portion of the incident-wave energy is transmitted. For example, $t_{-1}^{\rightarrow} = 0.14$ for $\mu = 0.7$ eV and $t_{-1}^{\rightarrow} = 8 \times 10^{-3}$ for $\mu = 0.01$ eV, when $f = 24.2$ THz, and $t_{-1}^{\rightarrow} = 0.048$ for $\mu = 0.01$ eV and $t_{-1}^{\rightarrow} = 2 \times 10^{-3}$ for $\mu = 0.7$ eV, when $f = 24.8$ THz. In contrast with the results of Fig. 4(a,b), in the vicinity of 24.5 THz, tunable deflection co-exists in Fig. 4(c,d) with tunable asymmetry in transmission, at which $t_0 \approx t_{-1}^{\leftarrow} \approx 0$. At the used values of $\mu$, we have here (nearly) total reflection for backward-case illumination, whereas for forward-case illumination we get either (nearly) total reflection, or deflection in transmission plus reflection, depending on the choice of $\mu$. An example of the field distribution is presented in Fig. 5.

The obtained results show that the capability of the graphene-dielectric metamaterial to work as a tunable element depends on its location with respect to other structural components. Indeed, from the comparison of Fig. 3(c,d) and Fig. 4(c,d) at 20 THz, it may be expected that it depends on whether the metamaterial slab directly affects phase and coupling conditions at the grating's interface, where unblocked transmission channel responsible for deflection is created (like in Fig. 4), or these conditions at a grating interface are not directly affected by the metamaterial slab (like in Fig. 3). A deeper study is needed to clarify the origin of this difference.

Since the studied structures are Lorentz-reciprocal, the incident and outgoing waves can be interchanged. In other words, as far as strong tunability was obtained, for instance, at $\phi_{-1} = -24.6°$ [Fig. 4(a)], it indicates that the tunable deflection is obtainable at smaller $\theta$ but larger $|\phi_{-1}|$ than in Figs. 3 and 4. Note that there is a wide choice of materials for the grating. In particular, the use of materials with smaller $\varepsilon_g$ than in Figs. 3 and 4 (e.g., $\varepsilon_g = 5.8$) can lead to stronger transmission in the deflection regime, with less sharp variations in transmission spectra, but at the price of weaker tunability. Therefore, a trade-off can be required at the design stage.

### 3.2. Structures without LiF slab

As seen in Figs. 1(c) and 4, efficient tunability of deflection is possible at $f = 24.5$ THz in the transparency regime, i.e., when $\mathrm{Re}(\varepsilon_{LiF})$ is close to 1 and $\mathrm{Im}(\varepsilon_{LiF})$ can be neglected. Therefore, the LiF slab can be *removed* in this case. Figure 6 presents $t_{-1}^{\rightarrow}$ and $t_{-1}^{\leftarrow}$ at $\theta = 60°$ for the *third configuration*, which differs from that one in Figs. 4 and 5 in that the LiF slab is removed. Behavior of $t_{-1}^{\rightarrow}$ in Fig. 6(a) is very similar to that one in Fig. 4(a) and Fig. 4(b), inset. Thus,

Optical Materials EXPRESS

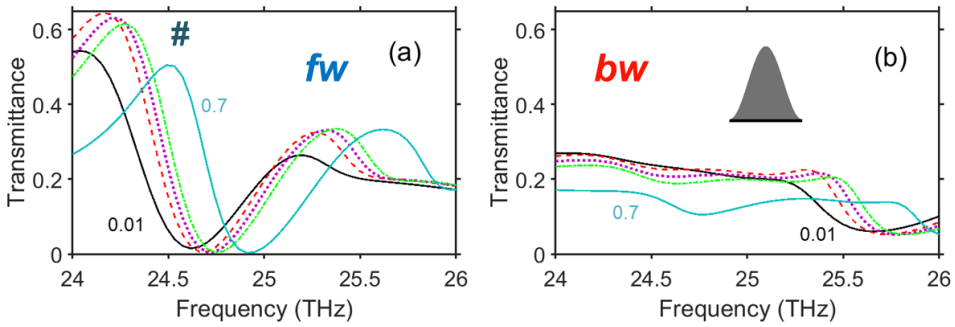


Fig. 6. (a) First-order forward-case transmittance, $t_{-1}^{\rightarrow}$, and (b) first-order backward-case transmittance, $t_{-1}^{\leftarrow}$ at $\theta = 60°$ in the vicinity of 25 THz; solid black line - $\mu = 0.01$ eV, dashed red line - $\mu = 0.162$ eV; dotted violet line - $\mu = 0.23$ eV; dash-dotted green line - $\mu = 0.3$ eV; solid light-blue line - $\mu = 0.7$ eV; *fw*, *bw*, number signs, and numbers near some of the curves have the same meaning as in Figs. 3 and 4.

the LiF slab only introduces some losses in this deflection scenario. However, asymmetry in transmission can be stronger due to its presence. It is noticeable that on-off switchable deflection is obtained here, while the metamaterial slab is placed not inside but at one of the interfaces of the entire structure. At the same time, modulation effect of the LiF slab in ENZ regime [33, 48] is absent for this structure, and the absence of this slab can make the resulting structure more feasible. Thus, one may expect more tuning scenarios at $f < 20$ THz, where propagation of the order $m = -1$ is already allowed by the grating theory [45] but here not suppressed, in contrast to the structures with the LiF slab, while the metamaterial is switchable from the dielectric to the plasmonic state by using the same range of $\mu$ variation. Clearly, there is no analog of the scenario observed in Figs. 3 and 4 for $\theta = 82°$ at 20 THz, but there is analog of that one obtained for $\theta = 82°$ at 24.5 THz (not shown).

Figure 7 presents $t_{-1}^{\rightarrow}$ and $t_{-1}^{\leftarrow}$ for the same structure as in Fig. 6, but at 17 THz, i.e., at the propagation threshold of the order $m = -1$. On the contrary to Figs. 3, 4, and 6, the efficient tuning of deflection does not need the use of $\mu = 0.01$ eV. Moreover, it is obtained for $t_{-1}^{\leftarrow}$, not for $t_{-1}^{\rightarrow}$. Such a scenario has not been found in the two above discussed structures with the LiF slab. Here, on-off switching of deflection is achieved together with tunable asymmetry in transmission, by varying $\mu$ from 0.3 eV to 0.7 eV. More than 18-fold difference in $t_{-1}^{\leftarrow}$ is obtained due to this variation, while $t_{-1}^{\rightarrow}$ is affected much weaker. At $f = 17.02$ THz ($\phi_{-1} = -79°$), we obtain $t_{-1}^{\leftarrow} = 0.375$ for $\mu = 0.3$ eV and $t_{-1}^{\rightarrow} = 0.02$ for $\mu = 0.7$ eV. In addition, strong asymmetry is achieved here for $\mu = 0.7$ eV, i.e., $t_{-1}^{\leftarrow}/t_{-1}^{\rightarrow} \approx 12$. Note that 5-fold difference in $t_{-1}^{\rightarrow}$ was obtained in the same structure at $\theta = 40°$ by varying $\mu$ from 0.3 eV to 0.7 eV for $f = 24.9$ THz ($\max t_{-1}^{\rightarrow} \approx 0.5$ at 0.7 eV, $\phi_{-1} = -38°$), while 4-fold difference was obtained for $f = 21$ THz ($\max t_{-1}^{\rightarrow} \approx 0.5$ at 0.3 eV, $\phi_{-1} = -58°$). Besides, on-off switching can be obtained without deflection and asymmetric transmission, owing to the order $m = 0$, as occurs, for instance, at $f = 16.25$ THz (not shown). In this case, $t_0 = 0.83$ for 0.162 eV and $t_0 = 0.05$ for 0.7 eV.

It is worth noting that although higher transmission efficiency for the order $m = -1$ and higher contrast between forward and backward transmission are, in general, more desirable, the use of a figure-of-merit might be contradictive with the goals of this work. It is important that the studied structures are not scalable, because conductivity of graphene and permittivity of LiF are not scalable. However, it should be possible to re-design these structures, at least for different parts of THz range. It can be done, in particular, by using other polar dielectrics than LiF (e.g., see Refs. [46, 52]), and other values of $d$ (see Eq. 5). Possible effects of grating shape and relaxation time of graphene on the scenarios of tunable deflection, and existence of the scenarios that may

Optical Materials EXPRESS

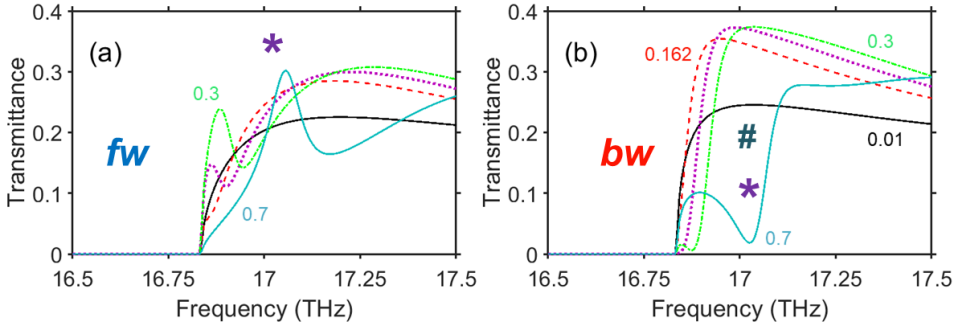


Fig. 7. Same as Fig. 6 but in the vicinity of 17 THz; asterisk sign has the same meaning as in Figs. 3 and 4.

need a narrower range of $\mu$ variation will be studied in another paper.

## 4. Conclusion

To summarize, we investigated diffractive deflection of linearly polarized terahertz waves by three- and two-component periodic structures that allow us to combine the effects of diffractions, ENZ-range dispersion, and transition from dielectric state to plasmonic state, in order to obtain tunable deflection and tunable asymmetric transmission. Based on the obtained results, at least four scenarios of tunable deflection can be distinguished. For the first of them, which requires ENZ regime for the LiF slab to suppress backward transmission due to the specific dispersion, the spectral location of the transmission maximum at the grating-side illumination is immune against variations in $\mu$, while transmittance is sensitive. The second scenario also needs ENZ regime for the LiF slab but now both transmittance and the maximum location are changeable. In these two scenarios, asymmetry in transmission is strong and well tunable. The third scenario of tunable deflection is realized when the LiF slab's permittivity is close to unity. This scenario results from an accidental effect of $\mu$ on diffraction, so that it has a fully diffractive nature. Clearly, it may have analog in the similar structure without the LiF slab. In such a simplified structure, one more, i.e., the fourth scenario has been found in the vicinity of the $m = -1$ order threshold. Compared to the first and second scenarios, it shows strong transmission for all of the used values of $\mu$, except for one of them, and this difference occurs only for one of the two opposite incidence directions. It also differs from the third scenario. Which of these scenarios can be realized depends on the choice of the incidence angle, $\theta$, frequency range, and location of the graphene-dielectric metamaterial slab. Performances operating at smaller $\theta$ can be re-designed for future experimental studies of the found deflection scenarios.

## Funding

Narodowe Centrum Nauki (NCN), Poland (DEC-2015/17/B/ST3/00118 – Metasel); TUBITAK (113E331, 114E374, 115F560); EU Horizon-2020 via Marie Sklodowska-Curie IF program (grant no. 708200 – ADVANTA); Ministerio de Economía, Industria y Competitividad, Spain (TEC2014-51902-C2-2-R).

## Acknowledgments

E.O. acknowledges partial support from the Turkish Academy of Sciences.

Optical Materials EXPRESS

## References


1. A. N. Grigorenko, M. Polini, and K. S. Novoselov, "Graphene plasmonics," Nat. Photon. **6**, 749–758 (2012).
2. A. K. Geim and K. S. Novoselov, "The rise of graphene," Nat. Mat. **6**, 183–191 (2007).
3. F. Bonaccorso, Z. Sun, T. Hasan, and A. C. Ferrari, "Graphene Photonics and Optoelectronics," Nat. Photon. **4**, 611–622 (2010).
4. L. A. Falkovsky, "Optical properties of graphene," J. Phys.: Conf. Ser. **129**(1), 012004 (2008).
5. Y. Yao, M. A. Kats, P. Gevenet, N. Yu, Y. Song, J. Kong, and F. Capasso, "Broad Electrical Tuning of Graphene-Loaded Plasmonic Antennas," Nano Lett. **13**(3), 1257-1264 (2013).
6. A. Yu. Nikitin, F. Guinea, and L. Martin-Moreno, "Resonant plasmonic effects in periodic graphene antidot arrays," Appl. Phys. Lett. **101**(15), 151119 (2012).
7. Z. Fang, Z. Liu, Y. Wang, P. M. Ajayan, P. Nordlander, and N. J. Halas, "Graphene-Antenna Sandwich Photodetector," Nano Lett. **12**(7), 3808–3813 (2012).
8. H. Hajian, I. D. Rukhlenko, P. T. Leung, H. Caglayan, and E. Ozbay, "Guided plasmon modes of a graphene-coated Kerr slab," Plasmonics **11**(3), 735–741 (2016).
9. A. N. Morozovska, A. I. Kurchak, and M. V. Strikha, "Graphene Exfoliation at a Ferroelectric Domain Wall Induced by the Piezoelectric Effect: Impact on the Conductance of the Graphene Channel," Phys. Rev. Appl. **8**(5), 054004 (2017).
10. D. Rodrigo, A. Tittl, O. Limaj, F. J. Garcia de Abajo, V. Pruneri, and H. Altug, "Double-layer graphene for enhanced tunable infrared plasmonics," Light: Sci. Appl. **6**, e16277 (2017).
11. I. Khromova, A. Andryieuski, and A. Lavrinenko, "Ultrasensitive terahertz/infrared waveguide modulators based on multilayer graphene metamaterials," Laser Photon. Rev. **8**(6), 916–923 (2014).
12. I. Crassee, J. Levallois, A. L. Walter, M. Ostler, A. Bostwick, E. Rotenberg, T. Seyller, D. van der Marel, and A. B. Kuzmenko, "Giant Faraday rotation in single- and multilayer graphene," Nat. Phys. **7**, 48–51 (2011).
13. H. Hajian, H. Caglayan, and E. Ozbay, "Long-range Tamm surface plasmons supported by graphene-dielectric metamaterials," J. Appl. Phys. **121**(3), 033101 (2017).
14. B. Orazbayev, M. Beruete, and I. Khromova, "Tunable beam steering enabled by graphene metamaterials," Opt. Express **24**(8), 8848–8861 (2016).
15. M. A. K. Othman, C. Guclu, and F. Capolino, "Graphene-dielectric composite metamaterials: evolution from elliptic to hyperbolic wavevector dispersion and the transverse epsilon-near-zero condition," J. Nanophoton. **7**(1), 073089 (2013).
16. M. A. K. Othman, C. Guclu, and F. Cappolino, "Graphene-based tunable hyperbolic metamaterials and enhanced near-field absorption," Opt. Express **21**(6), 7614–7632 (2013).
17. B. Zhu, G. Ren, S. Zheng, Z. Lin, and S. Jian, "Nanoscale dielectric-graphene-dielectric tunable infrared waveguide with ultrahigh refractive indices," Opt. Express **21**(14), 17089–17096 (2013).
18. Y. Xiang, J. Guo, X. Dai, S. Wen, and D. Tang, "Engineered surface Bloch waves in graphene-based hyperbolic metamaterials," Opt. Express **22**(3), 3054–3062 (2014).
19. I. V. Iorsh, I. S. Mukhin, I. V. Shadrinov, P. A. Belov, and Y. S. Kivshar, "Hyperbolic metamaterials based on multilayer graphene structures," Phys. Rev. B **87**(7), 075416 (2013).
20. Y. Xiang, X. Dai, J. Guo, H. Zhang, S. Wen, and D. Tang, "Critical coupling with graphene-based hyperbolic metamaterials," Sci. Rep. **4**, 5483 (2014).
21. T. Gric, "Surface-Plasmon-Polaritons at the Interface of Nanostructured Metamaterials," Prog. Electromag. Res. M **46**, 165–172 (2016).
22. T. Gric and O. Hess, "Tunable surface waves at the interface separating different graphene-dielectric composite hyperbolic metamaterials," Opt. Express **25**(10), 11466–11476 (2017).
23. J. Wu, L. Jiang, J. Guo, X. Dai, Y. Xiang, and S. Wen, "Tunable perfect absorption at infrared frequencies by a graphene-hBN hyper crystal," Opt. Express **24**(15), 17103–17114 (2016).
24. Y.-C. Chang, C.-H. Liu, C.-H. Liu, S. Zhang, S. R. Marder, E. E. Narimanov, Z. Zhong, and T. B. Norris, "Realization of mid-infrared graphene hyperbolic metamaterials," Nat. Commun. **7**, 10568 (2016).
25. C. Lu, X. Hu, Y. Zhang, Z. Li, X. Xu, et. al., "Ultralow power all-optical diode in photonic crystal heterostructures with broken spatial inversion symmetry," Appl. Phys. Lett. **99**(5), 051107 (2011).
26. A. E. Serebryannikov and A. Lakhtakia, "Wideband switchable unidirectional transmission in a photonic crystal with a periodically nonuniform pupil," Opt. Lett. **38**(17), 3279–3282 (2013).
27. F. T. Gundogdu, A. E. Serebryannikov, A. O. Cakmak, and E. Ozbay, "Asymmetric transmission in prisms using structures and materials with isotropic-type dispersion," Opt. Express **23**(19), 24120–24132 (2015).
28. T. Xu and H. J. Lezec, "Visible-frequency asymmetric transmission devices incorporating a hyperbolic metamaterial," Nat. Commun. **5**, 4141 (2016).
29. X.-F. Li, X. Ni, L. Feng, M.-H. Lu, C. He, and Y.-F. Chen, "Tunable Unidirectional Sound Propagation through a Sonic-Crystal-Based Acoustic Diode," Phys. Rev. Lett. **106**(8), 084301 (2011).
30. A. E. Serebryannikov and E. Ozbay, "One-way Rayleigh-Wood anomalies and tunable narrowband transmission in photonic crystal gratings with broken structural symmetry," Phys. Rev. A **87**(5), 053804 (2013).
31. L. Zinkiewicz, J. Haberko, and P. Wasylczyk, "Highly asymmetric near infrared light transmission in an all-dielectric grating-on-mirror photonic structure," Opt. Express **23**(4), 4206–4211 (2015).
32. M. J. Lockyear, A. P. Hibbins, K. R. White, and J. R. Sambles,"One-way diffraction grating," Phys. Rev. E **74**(5),

Optical Materials EXPRESS

056611 (2006).
33. A. E. Serebryannikov, E. Ozbay, and S. Nojima, "Asymmetric transmission of terahertz waves using polar dielectrics," Opt. Express **22**(3), 3075–3088 (2014).
34. A. E. Serebryannikov and E. Ozbay, "Unidirectional transmission in non-symmetric gratings containing metallic layers," Opt. Express **17**(16), 13335–13345 (2009).
35. P. Rodriguez-Ulibarri, M. Beruete, M. Navarro-Cia, and A. E. Serebryannikov, "Wideband unidirectional transmission with tunable sign-switchable refraction and deflection in nonsymmetric structures," Phys. Rev. B **88**(16), 165137 (2013).
36. P. Rodriguez-Ulibarri, V. Pacheco-Pena, M. Navarro-Cia, A. E. Serebryannikov, and M. Beruete, "Experimental demonstration of deflection angle tuning in unidirectional fishnet metamaterials at millimeter-waves," Appl. Phys. Lett. **106**(6), 061109 (2015).
37. Y. Fu, L. Xu, Z. H. Hang, and H. Chen, "Unidirectional transmission using array of zero-refractive-index metamaterials," Appl. Phys. Lett. **104**(19), 193509 (2014).
38. W.-M. Ye, X.-D. Yuan, C.-C. Guo, and C. Zen, "Unidirectional transmission in non-symmetric gratings made of isotropic material," Opt. Express **18**(8), 7590–7595 (2010).
39. H. Jiang, W. Zhao, and Y. Jiang, "High-efficiency tunable circular asymmetric transmission using dielectric metasurface integrated with graphene sheet," Opt. Express **25**(17), 19732–19739 (2017).
40. Y. Zhou, Y.-Q. Dong, R.-H. Fan, Q. Hu, R.-W. Peng, and M. Wang, "Asymmetric transmission of terahertz waves through a graphene-loaded metal grating," Appl. Phys. Lett. **105**(4), 041114 (2014).
41. Z. Li, W. Liu, H. Cheng, S. Chen, and J. Tian, "Tunable dual-band asymmetric transmission for circularly polarized waves with graphene planar chiral metasurfaces," Opt. Lett. **41**(13), 3142–3145 (2016).
42. J. Zhao, J. Zhang, Z. Zhu, X. Yuan, and S. Qin, "Tunable asymmetric transmission of THz wave through a graphene chiral metasurface," J. Opt. **18**(9), 095001 (2016).
43. Y. Huang, Z. Yao, F. Hu, C. Liu, L. Yu, Y. Lin, and X. Xu, "Tunable circular polarization conversion and asymmetric transmission of planar chiral graphene-metamaterial in terahertz region," Carbon **119**, 305–313 (2017).
44. T. Magath and A. E. Serebryannikov, "Fast iterative, coupled-integral-equation technique for inhomogeneous profiled and periodic slabs," J. Opt. Soc. Am. A **22**(11), 2405–2418 (2005).
45. R. Petit, Ed., *Electromagnetic Theory of Gratings* (Springer, 1980).
46. C. Kittel, *Introduction to Solid State Physics* (John Wiley and Sons, 2005).
47. A. E. Serebryannikov, S. Nojima, and E. Ozbay, "One-way absorption of terahertz waves in rod-type and multilayer structures containing polar dielectrics," Phys. Rev. B **90**(23), 235126 (2014).
48. S. Foteinopoulou, M. Kafesaki, E. N. Economou, and C. M. Soukoulis, "Two-dimensional polaritonic photonic crystals as terahertz uniaxial metamaterials," Phys. Rev. B **84**(3), 035128 (2011).
49. A. E. Serebryannikov, S. Nojima, K. B. Alici, and E. Ozbay, "Effect of in-material losses on terahertz absorption, transmission, and reflection in photonic crystals made of polar dielectrics," J. Appl. Phys. **118**(13), 133101 (2015).
50. G. C. R. Devarapu and S. Foteinopoulou, "Broadband Near-Unidirectional Absorption Enabled by Phonon-Polariton Resonances in SiC Micropyramid Arrays," Phys. Rev. Appl. **7** (3), 034001 (2017).
51. M. Kafesaki, A. A. Basharin, E. N. Economou, and C. M. Soukoulis, "THz metamaterials made of phonon-polariton materials," Photon. Nanostr. Fundam. Appl. **12**(4), 376–386 (2014).
52. R. I. Merino, M. F. Acosta, and V. M. Orera, "New polaritonic materials in the THz range made of directionally solidified halide eutectics," J. Eur. Ceram. Soc. **34**(9), 2061-2069 (2014).
53. J. S. Gomez-Diaz, C. Moldovan, S. Capdevila, J. Romeu, L. S. Bernard, A. Magrez, A. M. Ionescu, and J. Perruisseau-Carrier, "Self-biased reconfigurable graphene stacks for terahertz plasmonics," Nat. Commun. **6**, 6334 (2015).
54. A. E. Serebryannikov, K. B. Alici, T. Magath, A. O. Cakmak, and E. Ozbay, "Asymmetric Fabry-Perot-type transmission in photonic-crystal gratings with one-sided corrugations at a two-way coupling," Phys. Rev. A **86**(5), 053835 (2012).